BIOCHEMISTRY
including biophysical chemistry & molecular biology

Article

pubs.acs.org/biochemistry

Bacillus subtilis Class Ib Ribonucleotide Reductase: High Activity and Dynamic Subunit Interactions

Mackenzie J. Parker,[†] Xuling Zhu,[†,#] and JoAnne Stubbe*[,†,‡]

Departments of [†]Chemistry and [‡]Biology, Massachusetts Institute of Technology, 77 Massachusetts Avenue, Cambridge, Massachusetts 02139, United States

Supporting Information

ABSTRACT: The class Ib ribonucleotide reductase (RNR) isolated from *Bacillus subtilis* was recently purified as a 1:1 ratio of NrdE (α) and NrdF (β) subunits and determined to have a dimanganic-tyrosyl radical (Mn^{III}_2-Y·) cofactor. The activity of this RNR and the one reconstituted from recombinantly expressed NrdE and reconstituted Mn^{III}_2-Y· NrdF using dithiothreitol as the reductant, however, was low (160 nmol min^{-1} mg^{-1}). The apparent tight affinity between the two subunits, distinct from all class Ia RNRs, suggested that *B. subtilis* RNR might be the protein that yields to the elusive X-ray crystallographic characterization of an "active" RNR complex. We now report our efforts to optimize the activity of *B. subtilis* RNR by (1) isolation of NrdF with a homogeneous cofactor, and (2) identification and purification of the endogenous reductant(s). Goal one was achieved using anion exchange chromatography to separate apo-/mismetalated-NrdFs from Mn^{III}_2-Y· NrdF, yielding enzyme containing 4 Mn and 1 Y·/β_2. Goal two was achieved by cloning, expressing, and purifying TrxA (thioredoxin), YosR (a glutaredoxin-like thioredoxin), and TrxB (thioredoxin reductase). The success of both goals increased the specific activity to ~1250 nmol min^{-1} mg^{-1} using a 1:1 mixture of NrdE:Mn^{III}_2-Y· NrdF and either TrxA or YosR and TrxB. The quaternary structures of NrdE, NrdF, and NrdE:NrdF (1:1) were characterized by size exclusion chromatography and analytical ultracentrifugation. At physiological concentrations (~1 μM), NrdE is a monomer (α) and Mn^{III}_2-Y· NrdF is a dimer (β_2). A 1:1 mixture of NrdE:NrdF, however, is composed of a complex mixture of structures in contrast to expectations.

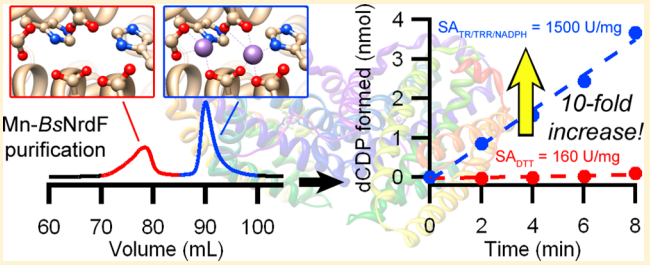

Ribonucleotide reductases (RNRs, Figure 1) catalyze the conversion of nucleoside 5′-diphosphates (NDPs) to deoxynucleotides (dNDPs) and play an essential role in supplying balanced dNTP pools for DNA replication and repair.[1] The RNRs have been classified based on the metallo-cofactors used to generate a transient cysteine thiyl radial that is essential for catalysis.[2] The class I RNRs contain two subunits (α and β) with subclassification (Ia, Ib, and Ic, Figure 1) based on the dimetallo-cofactor located in β. Class Ib RNRs, as with class Ia enzymes, were long thought to use a diferric-tyrosyl radical (Fe^{III}_2-Y·) cofactor because the cluster can self-assemble and has catalytic activity.[3−5] Recently however, the class Ib RNRs have been isolated and characterized from their endogenous sources (*Corynebacterium ammoniagenes*, *Escherichia coli*, and *Bacillus subtilis*) in sufficient amounts to establish that the cofactor is a dimanganic-tyrosyl radical (Mn^{III}_2-Y·).[6−9] While most prokaryotes have multiple RNRs, *B. subtilis* has a single essential class Ib RNR found in the *nrdI-nrdE-nrdF-ymaB* operon.[10−12] The apparent tight binding of the subunits of the *B. subtilis* RNR[9] and the low reported specific activities of this and other class Ib enzymes (Supporting Information, SI-Table 1), provided the impetus to maximize its catalytic activity for future structural determination.

In all class I RNRs, α (designated NrdE for class Ib and NrdA for class Ia, Figure 1) contains the active site for NDP reduction and binding sites for allosteric effectors that control substrate specificity.[1] The class Ia α contains a second allosteric site in its N-terminal ATP cone domain that controls the overall rate of nucleotide reduction and is absent in the class Ib α subunits. The β subunit (NrdF for class Ib and NrdB for class Ia) are all dimeric (β_2) with the class Ia housing a Fe^{III}_2-Y· cofactor (typically with 3.6 Fe/β_2 and 1 Y·/β_2) and the class Ib housing a Mn^{III}_2-Y·, whose stoichiometry remains to be optimized in all systems.[2]

Recent data suggest that in addition to allosteric effectors, quaternary structure(s) of the class I RNRs, including subunit affinity and its dependence on nucleotide binding, are all important in regulating RNR activity.[1] The subunit affinity in the *E. coli* and human class Ia RNRs have reported K_d's of ~0.2 μM in the presence of substrate (CDP)/effector (ATP).[13−15] While there is now a consensus that the active quaternary structure of *E. coli* class Ia RNR is $\alpha_2\beta_2$,[16−18] the eukaryotic Ia structure is open to debate [$(\alpha_2)_n(\beta_2)_m$ (n = 1, 3 and m = 1, 3)].[19−21] Recent studies have further revealed that the active complexes of both the prokaryotic and eukaryotic RNRs are dynamic.[16,17,21,22] The quaternary structures of the class Ib

Received: August 4, 2013
Revised: November 22, 2013
Published: January 8, 2014

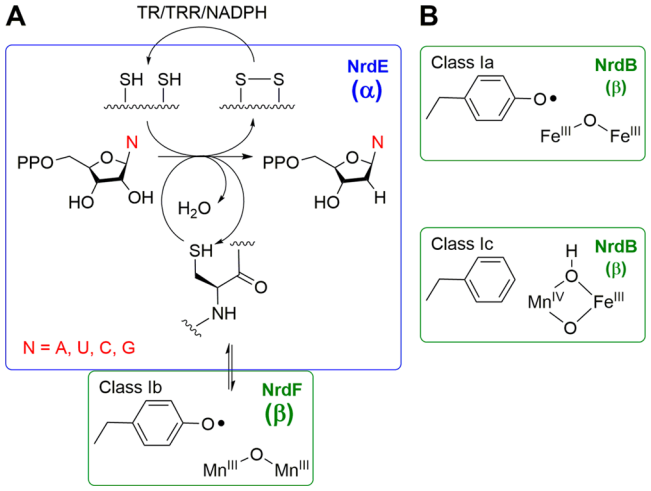

Figure 1. Ribonucleotide reduction catalyzed by class I RNRs. (A) The class Ib RNRs are composed of NrdE (α) and NrdF (β) which are proposed to form an $\alpha_2\beta_2$ complex during substrate turnover (only one α/β pair depicted). The stable dimaganic-Y· housed in β (1 Y·/β_2) oxidizes an essential Cys residue in the active site of α to a thiyl radical through a long-range radical transfer process involving redox-active amino acids in both subunits. Reduction of NDPs to dNDPs occurs concomitant with oxidation of two Cys residues to a disulfide. The disulfide is rereduced by a thioredoxin (TR) or NrdH (a glutaredoxin-like thioredoxin), thioredoxin reductase (TRR), and NADPH. (B) The dimetallo-cofactors of the class Ia and Ic β subunits.

RNRs, especially with the Mn^{III}_2-Y· cofactor, have been much less extensively studied and remain to be determined.[3,23,24]

Since the establishment that class Ib RNRs possess a Mn^{III}_2-Y· cofactor, many efforts have been made to isolate and characterize these enzymes.[6−9,23−25] With one exception[a], the reported activities of purified class Ib RNRs, whether endogenously or recombinantly sourced, are substantially lower (Supporting Information, SI-Table 1) than their class Ia counterparts (5000−8000 nmol min^{-1} mg^{-1}).[26] Recently our lab isolated the class Ib RNR from *B. subtilis* with NrdE and NrdF copurifying in a 1:1 ratio through three chromatographic steps in the absence of nucleotides and Mg^{2+}, suggesting "tight" subunit affinity.[9] However, while the RNR was 80% pure, its catalytic activity was low (~160 nmol min^{-1} mg^{-1}). Efforts to reconstitute active RNR using recombinantly expressed NrdE and reconstituted Mn^{III}_2-Y· NrdF also resulted in low catalytic activity.[9,27]

In this paper, we report optimization of the catalytic activity of the *B. subtilis* RNR by separation of active Me^{III}_2-Y· loaded-NrdF (Me = Fe or Mn) from the apo- and mismetalated forms and that the active form has 1 Y·/β_2 and 4 Mn/β_2. We also report the identification, cloning, expression, and purification of candidate genes for the endogenous reductants for *B. subtilis* RNR: TrxA and YosR, a thioredoxin and a glutaredoxin-like thioredoxin, respectively, and TrxB, a thioredoxin reductase. Activity assays with a 1:1 ratio of Mn^{III}_2-Y· NrdF:NrdE using either TrxA or YosR with TrxB gave specific activities of ~1250 nmol min^{-1} mg^{-1}, 7-fold higher activity than the Fe^{III}_2-Y· cofactor, and substantially higher than other class Ib RNRs (Supporting Information, SI-Table 1). A comparison of the ability of DTT versus the endogenous reductants to support RNR activity with purified or unpurified Mn^{III}_2-Y· NrdF revealed that the use of the endogenous reductants contributed significantly more to the activity enhancement relative to the cluster loading of NrdF. Activity assays with CDP/ATP and increasing concentrations of NrdE:NrdF maintained in a 1:1 ratio gave an apparent K_m of 25 nM, 10-fold lower than the apparent K_d for the Ia RNRs with the same substrate/effector pair.[13,14] The quaternary structure of each subunit and a 1:1 mixture of NrdE:NrdF at physiological concentrations (1 μM)[9] was examined by size exclusion chromatography (SEC) and sedimentation velocity analytical ultracentrifugation (SV-AUC) in the absence of nucleotides. These studies reveal that NrdE is a monomer, Me^{III}_2-Y· NrdF is a dimer, and the 1:1 mixture of NrdE and NrdF is a mixture of subunits and higher molecular weight species. These studies set the stage for determination of nucleotide binding and how it effects subunit interactions and quaternary structure in a class Ib RNR.

MATERIALS AND METHODS

Materials. Chemical reagents were obtained from Sigma-Aldrich at the highest purity available. Restriction enzymes, T4 DNA ligase, and isopropyl-β-D-1-thiogalactoside (IPTG) were purchased from Promega (Madison, WI). All DNA sequencing of cloned genes was carried out at the Massachusetts Institute of Technology Biopolymers Laboratory. Ni-NTA Fast Flow affinity resin was from Qiagen. Complete EDTA-free protease inhibitor tablets and calf alkaline phosphatase (20 μmol min^{-1} μL^{-1}) were purchased from Roche Biochemicals (Indianapolis, IN). Amicon Ultra-15 centrifugal filter devices were from Millipore. N-Terminally His_6-tagged NrdI and apo-NrdF were expressed and purified as reported previously.[9,27] Apo-NrdF was reconstituted with Mn^{III}_2-Y· and Fe^{III}_2-Y· as previously described.[9,28]

Cloning, Expression, and Purification of N-Terminally His_6-tagged TrxA, TrxB, and YosR. The genes *trxA*, *yosR*, and *trxB* were amplified by PCR using *B. subtilis* JH624 genomic DNA (a gift from A. Grossman in the Department of Biology, Massachusetts Institute of Technology) as a template and the primers listed in Supporting Information, SI-Table 2. The amplified DNA fragments were digested with NdeI and XhoI and ligated into pET14b (Novagen) using T4 DNA ligase to create the vectors pXZtrxA, pXZtrxB, and pXZyosR.

TrxA and YosR were overproduced from pXZtrxA and pXZyosR, respectively, transformed into BL21 (DE3) pLysS *E. coli* cells (Invitrogen). Cells were grown in 1 L of ampicillin-supplemented (Amp, 100 μg/mL) LB broth in 6 L Erlenmeyer flasks at 37 °C with 200 rpm shaking. At an OD_{600} of 0.8, IPTG was added to a final concentration of 0.2 mM and cultures were incubated for an additional 2 h before harvest. TrxB was overproduced from pXZtrxB transformed into BL21 (DE3) Codon Plus RIL-X *E. coli* cells (Agilent Technologies) following the same procedure with the exception that baffled 2.8 L Fernbach flasks were used for culture growth and incubation postinduction was extended to 3 h before harvest. Typical yields were 2.4−3.0 g cell paste L^{-1} for all strains.

The purification of all three proteins was the same through the nickel affinity step unless otherwise noted and was carried out at 4 °C. Cell pellets were thawed on ice and resuspended to 0.2 g paste mL^{-1} in buffer A (50 mM sodium phosphate, 300 mM NaCl, 10 mM imidazole, 5% (w/v) glycerol, pH 7.6) supplemented with protease inhibitors. Cells were lysed by passage through a French pressure cell at 14 000 psi and the debris was removed by centrifugation (35000*g*, 20 min). Streptomycin sulfate solution was added to the stirring cell extracts dropwise over 10 min to a final concentration of 1% (w/v). After an additional 15 min of stirring, precipitated

dx.doi.org/10.1021/bi401056e | *Biochemistry* 2014, 53, 766−776

materials were removed by centrifugation (35000*g*, 20 min). The streptomycin treatment was not used in the purification of TrxB as it caused precipitation of the desired protein. Clarified extracts were incubated with Ni-NTA resin equilibrated in buffer A for 1 h (1 mL of resin per 2.5 g of cell paste) on a rocker. The resin was then packed into a column and washed with 20 column volumes (CVs) of buffer B (50 mM sodium phosphate, 300 mM NaCl, 20 mM imidazole, 5% (w/v) glycerol, pH 7.6) before eluting protein with buffer C (50 mM sodium phosphate, 300 mM NaCl, 200 mM imidazole, 5% (w/v) glycerol, pH 7.6). Protein-containing fractions were identified using 15% SDS-PAGE gels and were then pooled and desalted on a Sephadex G-25 column with buffer D (50 mM sodium phosphate, 5% (w/v) glycerol, pH 7.6).

TrxA was purified further with a Sephadex G-75 column (41 × 2.5 cm, 0.25 mL min^{-1}) equilibrated with SEC buffer (50 mM sodium phosphate, 150 mM NaCl, pH 7.6). The fractions containing TrxA, assessed by SDS-PAGE, were pooled and desalted with an Amicon Ultra-15 YM-3 centrifugal filter (3000 MWCO). Typical yields were 11 ± 4 mg TrxA g^{-1} cell paste. Purity was assessed by 15% SDS-PAGE (Supporting Information, SI-Figure 1), and protein concentrations were estimated by ε_{280} of 12 700 M^{-1} cm^{-1} (DNASTAR Lasergene 8). The specific activity (SA) of the purified TrxA was ∼8−20 U/mg by the 5,5′-dithiobis-(2-nitrobenzoic acid) (DTNB) assay.[29,30]

YosR and TrxB were further purified by anion exchange chromatography on a BioCAD SPRINT FPLC system (PerSeptive Biosystems). Protein was loaded onto a Poros HQ/20 column (Applied Biosystems, 1.6 cm × 10 cm) equilibrated in AEX buffer (25 mM Tris, 5% (v/v) glycerol, pH 7.6) supplemented with 100 mM NaCl. The column was washed with 1 CV of equilibration buffer before development with a 100 mL linear gradient from 100 to 700 mM NaCl in AEX buffer. YosR eluted in the range of 350−450 mM NaCl (flow rate = 2 mL min^{-1}) and TrxB in the range of 230−280 mM NaCl (flow rate = 1 mL min^{-1}). Fractions containing TrxB were pooled by activity, exchanged to 50 mM NaPi, pH 7.6, 150 mM NaCl, and concentrated with an Amicon Ultra-15 YM30 centrifugal filter device (30000 MWCO). Fractions containing YosR, as assessed by 15% SDS-PAGE, were pooled, desalted, and concentrated with an Amicon Ultra-15 YM-3 centrifugal filter device. YosR was subjected to further purification using the SEC method described for TrxA. Typical yields were 3 mg YosR g^{-1} cell paste and 0.4 mg TrxB g^{-1} cell paste. Purity was assessed by 15% SDS-PAGE (Supporting Information, SI-Figure 1). The concentration of YosR was estimated by ε_{280} of 11 000 M^{-1} cm^{-1} (DNASTAR Lasergene 8). The concentration of TrxB was estimated with the BCA assay using BSA as a standard.[31] The FAD content of TrxB was determined as previously described.[32] SAs of YosR and TrxB of ∼20−26 U/mg and 415 U/mg, respectively, were determined using the DTNB assay.[29,30] One unit is defined as the amount of enzyme catalyzing a ΔA_{412} of 1.0 min^{-1}.[29,30]

Purification of NrdE. NrdE was purified as previously described except that buffer supplementation with NaCl and an additional anion exchange chromatographic step were introduced (see Supporting Information).[9]

Purification of holo-Me^{III}_2-Y· (Me = Fe or Mn) Subsequent to Cofactor Assembly. EDTA (pH 7.6) to a final concentration of 5 mM was added to 1 mL of reconstituted Me^{III}_2-Y· NrdF (40 μM Mn-loaded protein or 300 μM Fe-loaded protein, ∼0.6 Y·/β_2). Subsequent steps were at 4 °C. Samples were mixed, clarified by centrifugation (20817*g*, 2 min), and loaded onto a MonoQ 10/100GL anion exchange column (GE Healthcare, 10 × 1 cm) equilibrated with 50 mM Tris, pH 7.6, 5% (w/v) glycerol and 100 mM NaCl. The column was washed with 1.3 CVs of equilibration buffer before elution with a 100 mL linear gradient from 100 to 350 mM NaCl in Tris buffer at a flow rate of 1 mL min^{-1}. Apo-/mismetalated NrdF eluted at 250−280 mM NaCl (peak 1, Figure 2) and holo-protein at 280−310 mM (peak 2, Figure 2). Fractions (2 mL) containing protein were identified by A_{280}, and protein from each peak was pooled, exchanged into storage buffer (50 mM HEPES, 5% (w/v) glycerol, pH 7.6), and concentrated using Amicon Ultra-15 YM30 centrifugal filters. Typical yields were 35−45% of Mn^{III}_2-Y· NrdF and 53−63% of Fe^{III}_2-Y· NrdF. Pooled fractions were analyzed for metal content, Y· content, and activity as described subsequently.

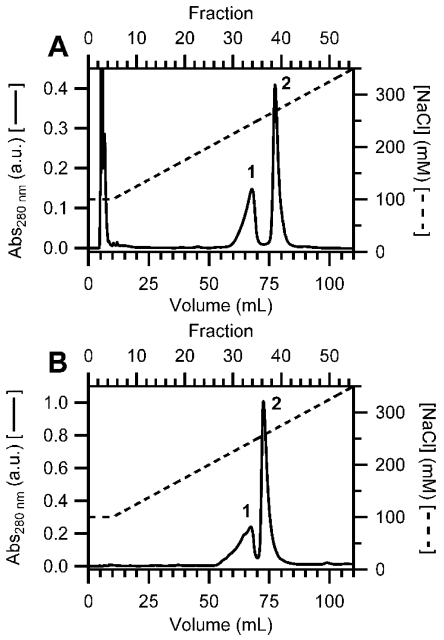

Figure 2. Separation of holo-Mn^{III}_2-Y· NrdF (A) and holo-Fe^{III}_2-Y· NrdF (B) from apo-/mis-metalated NrdFs by anion exchange chromatography on a MonoQ column. The material eluting in the void volume in (A) is $NrdI_{ox}$. Peak 1 corresponds to apo-/mis-metalated NrdF and 2 to holo-Me^{III}_2-Y· NrdF.

Metal Analysis of NrdF. Mn concentrations were determined using a Perkin-Elmer Analyst 600 atomic absorption spectrometer and a standardized Mn solution from Fluka. Iron concentrations were determined by the ferrozine assay.[33]

Y· Determination by EPR Spectroscopy. Spectra were acquired at 77 K on a Bruker EMX-X band spectrometer using a liquid N_2 finger dewar. Acquisition parameters for the Mn^{III}_2-Y· and Fe^{III}_2-Y· cofactors of NrdF were described previously.[34] Spin quantification was carried out by comparing the double integral of the signal intensity to that of a reference sample of *E. coli* NrdB (417 μM Y·, 1.2 Y·/β_2) as described previously.[34]

Activity Assays. Assays were carried out in a final volume of 200 μL containing: 0.5−1 μM Me^{III}_2-Y· NrdF (Me = Fe or Mn), 1 equiv of NrdE, 3 mM ATP, 1 mM [5-^{3}H]-CDP (ViTrax, specific activity ≈ 1100 cpm $nmol^{-1}$), reductant [8−20 mM DTT or 40 μM TrxA (8−20 U/mg) or YosR (20−26 U/mg), 0.4 μM TrxB (415 U/mg), and 1 mM NADPH], 50

mM HEPES, pH 7.6, 15 mM $MgCl_2$, and 1 mM EDTA at 37 °C. The reaction was initiated by addition of [5-^{3}H]-CDP. Aliquots (35 μL) were removed over 4 min and quenched by incubation at 100 °C for 2 min. The method of Steeper and Steuart was used to quantitate dCDP.[35] One unit of activity is the amount of enzyme required to catalyze 1 nmol dCDP min^{-1}. The effect of the allosteric effectors dATP (0.4 μM to 4 mM) or ATP (50 μM to 4 mM) on activity was carried out as described above.

The concentration dependence of RNR activity using a 1:1 mixture of α and β was measured with subunit ratios varying from 0.01−1 μM. At concentrations below 0.1 μM, BSA was included in the assay solution to a final concentration of 0.2 mg/mL. These data were fit to eq 1 with Igor Pro (Wavemetrics, Lake Oswego, OR).

$$\nu = \frac{V_{max}[\text{subunit}]}{K_m + [\text{subunit}]} \quad (1)$$

Quaternary Structural Analysis of 1:1 Mixtures of α:β Using Biophysical Methods. *A. Anion Exchange Chromatography.* NrdE and Me^{III}_2-Y· NrdF (Me = Fe or Mn, 1 Y·/β_2, ~3.6 Me^{3+}/β_2, 1450 U/mg [Mn^{III}_2-Y·] or 125 U/mg [Fe^{III}_2-Y·]) were mixed in a 1:1 ratio at 5 μM in 50 mM HEPES, 5% (w/v) glycerol, pH 7.6 in a total volume of 0.5−1 mL. Samples were incubated on ice for 20 min and at room temperature for 10 min, followed by centrifugation (20817*g*, 1 min, 4 °C). All subsequent steps were at 4 °C. Samples were injected onto a MonoQ anion exchange column equilibrated in 50 mM Tris, pH 7.6, 5% (w/v) glycerol and 100 mM NaCl. The column was washed with 1 CV of the equilibration buffer and then developed with a 160 mL linear gradient from 100 to 500 mM NaCl in Tris buffer at a flow rate of 1 mL min^{-1} (Supporting Information, SI-Figure 2). Fractions (2 mL) containing protein were identified by A_{280}, pooled, exchanged into storage buffer (50 mM HEPES, pH 7.6, 5% (w/v) glycerol), and concentrated using an Amicon Ultra-15 YM30 centrifugal filter. The metal content, radical content, and activity of the isolated complex was measured as described above.

B. SEC. Samples of NrdE (3 μM), holo-Fe^{III}_2-Y· NrdF (23 μM), holo-Mn^{III}_2-Y· NrdF (1 μM), and 1:1 mixtures of α:β (1 μM) in a total volume of 200 μL were centrifuged (20817*g*, 10 min, 4 °C) and then injected onto a Superdex 200 10/300 GL column (10 × 300 mm, ~24 mL) connected to an ÄKTA Purifier FPLC system (GE Healthcare). Protein was eluted at 4 °C at a flow rate of 0.25 mL min^{-1} using 50 mM HEPES, pH 7.6, 100 mM NaCl, 15 mM $MgCl_2$, 1 mM EDTA. Molecular weights were calculated as previously described[36] using the experimentally measured $s_{20,w}$ (subsequent section), the Stokes radius (R_s) estimated from the SEC retention times, and the correlation function of Laurent and Killander.[37] The column was calibrated using a High Molecular Weight Gel Filtration kit (GE Healthcare) containing the following standards: Blue Dextran 2000 (void volume determination), thyroglobulin (669 kDa, R_s = 85.0 Å), ferritin (440 kDa, R_s = 61.0 Å), aldolase (158 kDa, R_s = 48.1 Å), conalbumin (75 kDa, R_s = 36.4 Å[38]), and ovalbumin (44 kDa, R_s = 30.5 Å).

C. SV-AUC−Experimental Design. Concentration-dependent SV experiments were performed using a Beckman XL-I analytical ultracentrifuge at the MIT Biophysical Instrumentation Facility with Fe-β_2 (1.2 Y·/β_2, 4.0 Fe/β_2, 130 U/mg), Mn-β_2 (0.9 Y·/β_2, 4.0 Mn/β_2, 1545 U/mg), and α. Individual subunits were analyzed in 50 mM Tris, pH 7.6, 5% (w/v) glycerol, 150 mM NaCl, 15 mM $MgCl_2$, 1 mM DTT, whereas 1:1 mixtures of α and β were analyzed in 50 mM NaP_i, pH 7.6, 150 mM NaCl, 5% (w/v) glycerol, 1 mM TCEP to allow experiments to be monitored by A_{230}. Protein was exchanged into buffer using three cycles of concentration-dilution with an Amicon Ultra-15 YM30 centrifugal filter. The final filtrate was used as the SV reference buffer. Samples spanning 0.1−1.5 OD at A_{230}, A_{250}, or A_{280} (Supporting Information, SI-Table 3) were prepared in a total volume of 500 μL by mixing concentrated protein solution with reference buffer to the desired final concentration for each experiment. Epon charcoal double sector cells (12 mm) assembled with quartz windows were loaded with ~440 μL reference solution and ~430 μL sample solution, radially calibrated, and thermally equilibrated at 20 °C for 1.5−2.0 h prior to initiating the experiment. Sedimentation was measured over 18−19 h with absorption detection at 20 °C and an angular velocity of 35 000 rpm. Scans were collected every 1.2 min using ProteomeLab XL-I Graphical User Interface, version 4.5b (Beckman).[39]

C.1. Analysis Method. Individual data sets were fit with the c(s) model implemented in Sedfit with a resolution (N) = 200−250, and a regularization factor (P) = 0.95.[40,41] Distributions were converted to the standard state ($s_{20,w}$) using a solvent density (ρ) = 1.018 g mL^{-1} (Tris buffer) or 1.023 g mL^{-1} (NaP_i buffer), solvent viscosity (η) = 1.164 cP (Tris buffer) or 1.170 cP (NaP_i buffer), and the partial specific volume ($\bar{\nu}$) of the species analyzed (Supporting Information, SI-Table 4); these values were calculated and temperature corrected with Sednterp.[42] All Mn^{III}_2-Y· NrdF data sets and the NrdE and NrdE:Fe^{III}_2-Y· NrdF data collected at physiological concentrations (~1 μM) were fit with the program Sedphat using the "hybrid local continuous/global discrete species model" for a more rigorous determination of $s_{20,w}$ and M_w.[40] The best fit $s_{20,w}$ for each species was used to determine R_s and the frictional ratio (f/f_o) with Sednterp by turning off the temperature corrections, setting ρ = 0.998 g mL^{-1} and η = 1.002 cP, and calculating the M_w values using the amino acid sequences of NrdE and NrdF (including the His-tag).

D. Hydrodynamic Modeling. Predictions of the $s_{20,w}$, frictional ratio (f/f_o), and R_s for each species were determined using the program HYDROPRO[43] and structural models of NrdE and NrdF (PDB 4DRO) (Supporting Information, SI-Table 4).[44] A crystallographic structure of *B. subtilis* NrdE is not available, and therefore the web-based server PHYRE[45] was used to generate a NrdE model by threading onto the *Salmonella typhimurium* NrdE structure (PDB 1PEM, 45% identity to *B. subtilis* NrdE; see Supporting Information).[46]

SDS-PAGE Densitometry. The ratio of α:β in 1:1 mixtures was estimated by densitometry using standard curves prepared from known amounts of NrdE and NrdF as described previously.[9] See Supporting Information for details.

RESULTS

Purification of Me^{III}_2-Y· NrdF (Me = Fe or Mn) to give 1 Y·/β_2. The low amounts of Y· and metal content in class Ib β subunits examined to date suggest that NrdFs (Supporting Information, SI-Table 1) are heterogeneous mixtures of holo- and apo-/mismetalated protein. On the basis of the report of partial separation of *Bacillus anthracis* holo- and apo-NrdF,[24] *B. subtilis* NrdF was examined on different anion exchange resins with MonoQ ultimately effecting complete separation of holo-Fe-β_2 and Mn-β_2 from apo-/mismetalated-NrdF (Figure 2). Analysis of pooled peak 2 by atomic absorption and EPR

spectroscopy revealed 4.1 ± 0.3 Mn/β_2 and 1.00 ± 0.09 Y·/β_2 for Mn^{III}_2-Y· NrdF and by ferrozine assay and EPR spectroscopy 4.0 ± 0.1 Fe/β_2 and 1.05 ± 0.05 Y·/β_2 for Fe^{III}_2Y· NrdF (Supporting Information, SI-Figure 3). In contrast, pooled protein from peak 1 (Figure 2) typically had 0.1 Y·/β_2, ~1.0 metal/β_2, and no detectable activity. Holo-NrdF from peak 2 has been used in all subsequent experiments.

Purification of *B. subtilis* TrxA, YosR, and TrxB. The highest activities of class I RNRs have been achieved with endogenous reducing systems that are distinct for different class Ib RNRs (see Supporting Information, SI-Table 1).[25] Mining of *B. subtilis* JH624 genome revealed a number of candidate genes. Thioredoxin (*trxA*, TR), YosR (*yosR*, a NrdH or glutaredoxin-like thioredoxin[25,47]), and thioredoxin reductase (*trxB*, TRR) were ultimately pursued due to homology to the reductants that maximally supported RNR activity in *B. anthracis*.[9,25] His-tagged versions of these genes were cloned, overexpressed in *E. coli*, and purified by Ni-affinity chromatography. Each protein required additional purification steps. For TrxA, Sephadex G-75 SEC yielded ≥99% pure protein (Supporting Information, SI-Figure 1) with a specific activity of ~11−20 U/mg using the DTNB assay in the presence of NADPH and TrxB. For YosR, Poros HQ/20 FPLC anion exchange chromatography followed by Sephadex G-75 SEC resulted in ≥95% pure protein (Supporting Information, SI-Figure 1) with a specific activity of ~20−26 U/mg. Finally, nearly homogeneous TrxB with a full complement of FAD was obtained with Poros HQ/20 anion exchange (≥95% pure, Supporting Information, SI-Figure 1) and had a specific activity of 415 U/mg in the presence of either TrxA or YosR.

Assay Optimization. Historically, the activity of each subunit for class Ia RNRs has been assayed independently in the presence of an excess of the second subunit due to weak subunit interactions.[26,48] Similar assays of Ib RNRs have been carried out using this protocol.[3,5,8,9,24,34,49] Our previous results, however, suggested the *B. subtilis* RNR could be assayed as a holo-enzyme by using equivalent amounts of each subunit.[9] To validate the use of a 1:1 ratio of subunits, experiments were therefore initially carried out using 0.5−1 μM NrdF, increasing amounts of NrdE (1, 5, or 10 equiv), 3 mM ATP, and the endogenous reductants TrxA/TrxB/NADPH. The results with both Fe- and Mn-loaded NrdF in a 1:1 ratio with NrdE gave activity very similar to that in the presence of a 5−10-fold excess of NrdE (data not shown). Thus, all further studies used a 1:1 ratio of the subunits.

Optimization of Effector (ATP, dATP) Concentrations. Previous studies of the Fe-loaded *S. typhimurium*, *Lactococcus lactis*, and *Mycobacterium tuberculosis* class Ib RNRs reported that dATP strongly stimulated CDP reduction, while ATP had only a marginal stimulatory affect.[3,5,49,50] These results contrast with the class Ia RNRs, in which dATP stimulates activity by binding to the specificity site of α at low concentrations and inhibits at high concentrations by binding to both the specificity and activity site leading to an $\alpha_4\beta_4$ inhibitory complex.[16,18] This quaternary structure is inaccessible in Ib RNRs as they lack the ATP cone domain essential for $\alpha_4\beta_4$ formation.[22] Thus, studies with both ATP and dATP were carried out, and the results are shown in Figure 3. ATP maximally stimulated CDP reduction at 1.5−2 mM, while dATP showed maximal stimulation at 8−10 μM followed by rapid inhibition at higher concentrations. The effects were similar with Fe-loaded NrdF (data not shown), although the activity was 5-fold lower. The dATP behavior was unexpected as there is no ATP cone domain, and it is distinct from other reported class Ib enzymes.[3,5,49,50] The Mg^{2+} dependence was also examined and gave an optimum activity at 10−15 mM, while EDTA had no effect on the activity (data not shown).

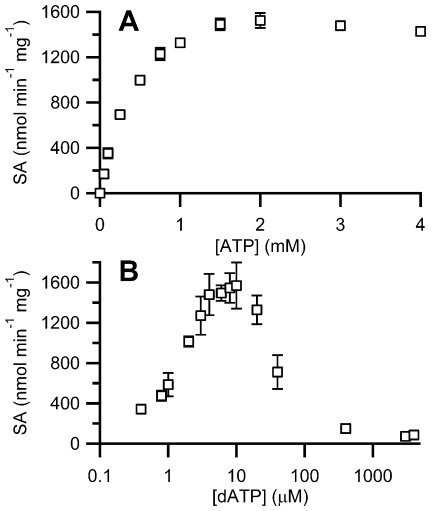

Figure 3. Effector nucleotide concentration-dependence of CDP reduction by a 1:1 mixture of Mn^{III}_2-Y· NrdF and NrdE. Assays were conducted with 0.5 μM of each subunit. Error bars represent ±1 standard deviation from the mean. (A) Dependence of *B. subtilis* RNR activity on ATP. (B) Dependence of *B. subtilis* RNR activity on dATP.

The SA of *B. subtilis* RNR under optimized conditions with CDP/(d)ATP is among the highest reported for any member of this subclass (Table 1; Supporting Information, SI-Table 1).

Table 1. Optimized CDP Reduction Activity of *B. subtilis* NrdF[a]

Me	reductant[b]	effector	SA (U/mg)
Fe	DTT	3 mM ATP	52 ± 3
		1 mM ATP	22[c]
	TrxA	3 mM ATP	125 ± 23
			86 ± 5[d]
	YosR	3 mM ATP	106 ± 8
	TrxA	4 μM dATP	172 ± 22
Mn	DTT	3 mM ATP	146 ± 14
		1 mM ATP	160[c]
	TrxA	3 mM ATP	1475 ± 129
			721 ± 128[e]
	YosR	3 mM ATP	997 ± 9
	TrxA	7 μM dATP	1257 ± 128

[a]Purified Me^{III}_2-Y· NrdF characteristics: Fe-β_2 = 1.1 Y·/β_2, 3.6 Fe/β_2; Mn-β_2 = 1.0 Y·/β_2, 3.2 Mn/β_2. [b]DTT, final concentration 20 mM. TrxA or YosR, the final concentration 40 μM and assays included 0.4 μM TrxB and 1 mM NADPH. [c]Previous study.[9] [d]Unpurified Fe^{III}_2-Y· NrdF (0.5 Y·/β_2, 2.8 Fe/β_2). [e]Unpurified Mn^{III}_2-Y· NrdF (0.6 Y·/β_2, 2.6 Mn/β_2).

Holo-Mn^{III}_2-Y· and Fe^{III}_2-Y· NrdF gave, respectively, 1475 ± 129 and 125 ± 23 U/mg with TrxA and 997 ± 9 U/mg and 106 ± 8 U/mg with YosR (Table 1). Given that we believe both cluster loading and reductant identity are important contributors to RNR activity, we compared the activities of purified and unpurified Me^{III}_2-Y· NrdF using both DTT and TrxA/TrxB/NADPH to establish the relative contributions of each factor to the overall activity enhancement observed with *B. subtilis* RNR. Surprisingly, the use of the endogenous reducing

system had a much greater effect on activity (5−10-fold enhancement with Mn^{III}_2-Y·) than did cluster assembly (0−2-fold enhancement, Table 1). This starkly contrasts with the *B. anthracis* RNR, where similar activities were observed with DTT and Trx1.[25]

Reconstitution of Active RNR from Recombinant NrdE and Reconstituted NrdF. The most distinct aspect of the copurification of endogenous NrdE and NrdF was that the complex was maintained in the absence of substrates, effectors, and Mg^{2+}.[9] Analysis of a 1:1 mixture NrdE:NrdF (5 μM) on a MonoQ FPLC column reproduced this result (Supporting Information, SI-Figure 2). A single peak eluted between 380−410 mM NaCl, behavior distinct from NrdE alone (two peaks that eluted between 265−300 mM NaCl and 325−340 mM NaCl) and reconstituted NrdF (two peaks that eluted in the range of 250−280 mM NaCl and 280−310 mM NaCl) using the same NaCl gradient. SDS-PAGE densitometry analysis of the fractions showed a 1:1 subunit ratio (Supporting Information, SI-Figure 4). Both the recovered Fe- and Mn-loaded complexes were active in CDP reduction (116 ± 5 U/mg and 889 ± 6 U/mg, respectively) and contained a nearly full complement of metal (Fe/β_2 = 3.8 ± 0.2; Mn/β_2 = 3.8 ± 1.6) and Y· (Fe-β_2 = 1.2 Y·/β_2, Mn-β_2 = 0.7 Y·/β_2).

***K*$_m$ for *α*/*β* Interaction.** Recent Western blot analysis of wild type *B. subtilis* JH624 using antibodies to NrdE and NrdF revealed that the two proteins were present in the crude cell extracts in a 1:1 subunit ratio at ∼1 μM.[9] Thus, CDP reductase activity using a 1:1 subunit ratio was examined with subunit concentrations that ranged from 0.01 μM to 1 μM in the presence of ATP (3 mM) and TrxA/TrxB/NADPH. The results are shown in Figure 4. Fitting the data to eq 1 gave V_{max} = 124 ± 6 U/mg and K_m = 0.06 ± 0.01 μM for Fe-β_2 and V_{max} = 1081 ± 36 U/mg and K_m = 0.025 ± 0.003 μM for Mn-β_2. The apparent affinity between the subunits is ∼10× greater than for the class Ia RNRs and the *B. anthracis* class Ib RNR.[13,23,24]

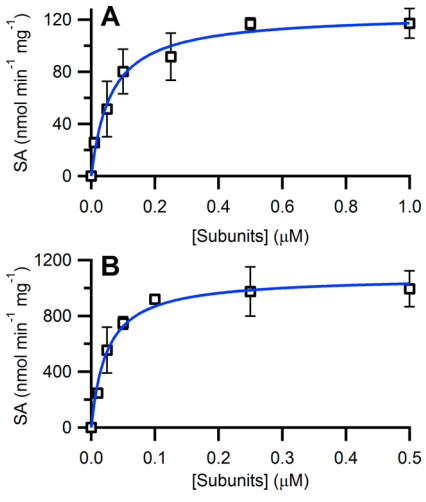

Figure 4. Subunit concentration dependence of activity of a 1:1 mixture of NrdE:Fe^{III}_2-Y· NrdF (A), or NrdE:Mn^{III}_2-Y· NrdF (B). Assay conditions include 1 mM CDP, 3 mM ATP, and optimized concentrations of TrxA/TrxB/NADPH. Error bars represent ±1 standard deviation from the mean. Blue lines are the fits of the data to eq 1, yielding (A) V_{max} =124 ± 6 nmol min^{-1} mg^{-1} and K_m = 0.062 ± 0.012 μM dATP, and (B) V_{max} = 1081 ± 36 nmol min^{-1} mg^{-1} and K_m = 0.025 ± 0.003 μM dATP.

Quaternary Structure by SEC. SEC was used initially to estimate the molecular weights of the subunits and quaternary structure(s) of holo-RNR. When run at physiological concentrations (∼1 μM), NrdF (Fe- or Mn-loaded) eluted predominantly as a single peak (Figure 5A) with a molecular

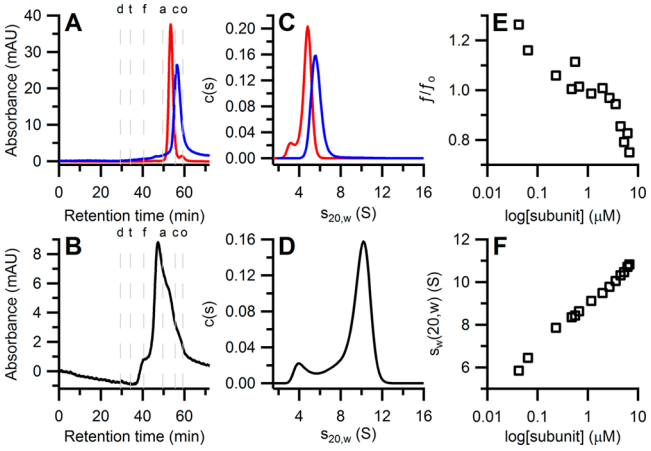

Figure 5. Biophysical characterization of the *B. subtilis* class Ib RNR (all at 1 μM) in the absence of nucleotides. (A) Overlaid SEC chromatograms of holo-Mn^{III}_2-Y· NrdF (red trace) and NrdE (blue trace). (B) SEC chromatogram of a 1:1 mixture of Mn^{III}_2-Y· NrdF:NrdE. Letters above the chromatograms indicate the retention time of molecular weight standards (*d* = Blue dextran 2000, *t* = thyroglobulin, *f* = ferritin, *a* = aldolase, *c* = conalbumin, *o* = ovalbumin). (C) Overlaid $s_{20,w}$ distributions of holo-Mn^{III}_2-Y· NrdF (red trace) and NrdE (blue trace). (D) The $s_{20,w}$ distribution of a 1:1 mixture of Fe^{III}_2-Y· NrdF:NrdE. (E) A plot of the weight averaged frictional ratios versus loading concentration of 1:1 mixture of Fe^{III}_2-Y· NrdF:NrdE shows a steep decrease as the subunit concentrations increase.[40] (F) An isotherm plotting the weight averaged $s_{20,w}$ against loading concentration of 1:1 mixtures of Fe^{III}_2-Y· NrdF:NrdE indicates complicated quaternary structural dynamics of the *B. subtilis* class Ib RNR.

weight of 80.1 kDa (Table 2), consistent with a dimer. A small amount of monomer was also observed (49.6 kDa, Table 2). NrdE also eluted as a single peak (Figure 5A) with a molecular weight of 82.7 kDa (Table 2), consistent with a monomer. The results with holo-RNR are shown in Figure 5B. The chromatogram reveals a series of broad peaks with retention times ranging from 37−60 min, indicating the presence of interconverting species. Regardless of the metal loading, the highest percentage of protein eluted at V_e = 47 min, corresponding to a molecular weight of 204.6 kDa (Table 2), suggesting, in conjunction with the other hydrodynamic properties, the presence of an $\alpha_2\beta_2$-like complex with a structure similar to the elongated *S. typhimurium* class Ib holo-RNR (Table 2).[51] However, these results clearly indicate that the quaternary structure(s) of the *B. subtilis* class Ib RNR are not stable in the absence of substrate or effector nucleotides, resulting in an ensemble of different interconverting species, despite the low experimentally measured K_m (Figure 4).

Quaternary Structure by SV-AUC. SV experiments with each subunit and with a 1:1 mixture of subunits were carried out at different concentrations (Supporting Information, SI-Table 3) to gain further insight into their quaternary states. To aid in the analysis of our experimental data, HYDROPRO[43] was used to predict hydrodynamic properties for NrdF and NrdE

Table 2. Biophysical Characteristics of *B. subtilis* Class Ib RNR in the Absence of Effectors[a]

	NrdE (1 μM)		Mn^{III}_2-Y· NrdF (1 μM)				1:1 NrdE:Fe^{III}_2-Y· NrdF (1 μM)			
sample	meas	pred	meas	pred	meas	pred	meas	pred	meas	pred
M_w (kDa)	71.4	83.0	35.4	40.6	94.2	81.3	30.8	40.6	199.2	247.2
	82.7		*49.6*		*80.1*				*204.6*	
$s_{20,w}$ (S)	5.56	5.37	3.64	3.47	4.72	5.51	3.64	3.47	9.59	10.8[b]
										11.4[c]
f/f_o	1.23	1.27	1.15	1.20	1.40	1.20	1.15	1.20	1.46	1.30[b]
	1.22		*1.40*		*1.38*				*1.21*	1.23[c]
R_s (Å)	35.4	36.4	26.1	27.2	40.1	34.6	26.1	27.2	60.9	54.0[b]
	35.3		*31.9*		*39.6*				*50.4*	51.2[c]
state(s)	α		β		β_2		β		$\alpha_n(\beta_2)_m$	

[a]Values derived from fits of the SV-AUC in Sedphat (regular font) and from the SEC data (italicized font) using the $s_{20,w}$ values determined by AUC. [b]Predicted values from HYDROPRO based on alignment of the *B. subtilis* class Ib RNR with the *S. typhimurium* class Ib holo-RNR.[51] [c]Predicted values from HYDROPRO based on alignment of the *B. subtilis* class Ib RNR with the *E. coli* class Ia docking model.[52]

from the NrdF crystal structure (PDB 4DRO)[44] and a threading model of NrdE using the *S. typhimurium* NrdE structure (PDB 1PEM).[46] Predictions were also made for docking models of the *B. subtilis* $\alpha_2\beta_2$ complex prepared by *in silico* alignment of the subunit models with the *E. coli* class Ia RNR globular docking model and the elongated X-ray structure of the *S. typhimurium* class Ib holo-RNR.[51,52] The results of the HYDROPRO calculations are summarized in Supporting Information, SI-Table 4.

The sedimentation behavior of Mn^{III}_2-Y· NrdF (1−11 μM), NrdE (1−30 μM), and NrdE:Fe^{III}_2-Y· NrdF (25 nM to 7 μM) were determined and analyzed using the c(s) model in Sedfit and, due to the detection by the c(s) fits of interactions occurring on the time scale of sedimentation, with Sedphat. The details of these analyses are presented in the Supporting Information and in SI-Figures 5−7. The results for 1 μM Mn^{III}_2-Y· NrdF are shown in Figure 5C and reveal two peaks representing stable, noninteracting entities at all concentrations examined (Supporting Information, SI-Figure 5). Globally fitting the data sets in Sedphat yielded $s_{20,w}$ = 3.64 and 4.72 S for each entity, along with the corresponding M_w's listed in Table 2. These results, in comparison with HYDROPRO predictions (Supporting Information, SI-Table 4) and SEC results (Table 2), suggest that the predominant species is a dimer and the minor species is a monomer. These results are consistent with the general reports that all class I small subunits are dimers.

The results of similar experiments with NrdE are shown in Figure 5C and Supporting Information, SI-Figure 6. At 1 μM NrdE, a single peak with an $s_{20,w}$ = 5.56 S is observed. However, analysis of increasing protein concentrations to 9 μM reveal a second peak at $s_{20,w}$ = 7.40 S (Supporting Information, SI-Figure 6A) and at still higher concentrations (30 μM), larger oligomeric states (Supporting Information, SI-Figure 6B). Thus, NrdE is in a regime where the protein is not stable and aggregates on the time scale of our experiments. The NrdE data analyzed in Sedphat, when compared to the HYDROPRO predictions (Supporting Information, SI-Table 4) and our SEC data (Table 2), suggest that the peak at low concentrations is the NrdE monomer. As the protein concentration increases NrdE appears to form a dimer that is unstable and continues to aggregate (Supporting Information, SI-Figure 6). We note that α, in prokaryotic and eukaryotic class Ia RNRs, in general exhibits low solubility and that aggregation has been reported by SAXS and EM analyses.[16] However, ours is the first systematic report of the complexity of α aggregation.

The analysis of a 1:1 mixture NrdE:Fe^{III}_2-Y· NrdF using c(s) is shown in Figure 5D (also see Supporting Information, SI-Figure 7). Even at 1 μM, dynamic behavior of the subunits is indicated by the reaction boundary that has apparent peaks at 4.38 and 9.66 S. A plot of the best fit f/f_o from the c(s) models versus loading concentration (Figure 5E) reveals a sharp decrease as the protein concentration increases. As described in more detail in the Supporting Information, this observation indicates the presence of interconverting species. The data were imported into Sedphat, and the peaks were treated as discrete species with individual f/f_o.[40] The calculated hydrodynamic properties of the smaller species ($s_{20,w}$ = 3.64 S) are consistent with a NrdF monomer. For the larger species ($s_{20,w}$ = 9.59 S), the analysis suggests the presence of oligomeric structures that are similar to, but smaller than, that predicted for an $\alpha_2\beta_2$ complex (Supporting Information, SI-Table 4). As noted however, this is clearly not a discrete species as this peak shifts to larger $s_{20,w}$, and larger complex(es) of unknown composition become evident as the protein concentration increases (Figure 5F, Supporting Information, SI-Figure 7). Thus, we currently do not have a model for the behavior of the 1:1 NrdE:NrdF complex. Further analysis requires the presence of different substrate and effector pairs after their binding stoichiometries are established and requires development of a method to specifically reduce the Y· in NrdF to prevent chemistry during the analysis.[34]

DISCUSSION

In 2010, it was shown that class Ib RNRs can assembly a Mn^{III}_2-Y· cofactor with the aid of the unusual flavodoxin NrdI and O_2 *in vitro*[34] and that enzymes isolated from three endogenous sources have a similar cluster.[6,7,9] More recently, *in vitro* assembly of a Mn^{III}_2-Y· cofactor using species specific NrdIs have been carried out in *B. subtilis*,[9,27] *Streptococcus sanguinis*,[53] *B. anthracis*, and *B. cereus*[24] with similar results. The interesting observation that a Fe^{III}_2-Y· cofactor can self-assemble in these enzymes *in vitro* and maintain catalytic activity, although demonstrably lower than the Mn-loaded cofactor (Supporting Information, SI-Table 1),[3−5,46,51] raises important biological questions as to the nature of the active cofactor *in vivo* and whether it changes with the growth conditions of the organism. Given that many pathogenic organisms [54] require a class Ib RNR for aerobic growth and that humans use a Fe^{III}_2-Y· class Ia RNR, the distinctions in the mechanisms of cofactor biosynthesis, allosteric regulation, and quaternary structure offer new opportunities for therapeutic intervention. Thus, understanding

the basic properties of the Ib RNRs, as well as their similarities and differences to one another and to class Ia RNRs, is an important first step.

Recent studies on the class Ib RNRs (with the Mn^{III}_2-Y· NrdF) from *B. anthracis* and *B. cereus* have identified and characterized the endogenous reductants required to make deoxynucleotides at optimum rates.[24,25] Despite this important contribution, however, these and other class Ib RNRs (Supporting Information, SI-Table 1) still have low catalytic activity. The *B. anthracis* Mn^{III}_2-Y· NrdF assembled with NrdI gave 0.3−0.4 Y·/β_2, but the reported activity was only 44−70 U/mg.[24,25] Similar activities were observed using DTT (40−63 U/mg) alone or with either TR or NrdH.[24,25] The *B. anthracis* Fe^{III}_2-Y· NrdF with 0.6 Y·/β_2 was reported to have activity of only 8 U/mg.[24] This value is very low given the high Y· content, which in the case of the Ia RNRs, is correlated with activity.[55] Our initial report on the activity of endogenous *B. subtilis* RNR using DTT as reductant was also low, 160 U/mg. To study the class Ib RNRs, we thus felt that we needed to better understand the basis for the low catalytic activity, which we believed to lie with cluster assembly in NrdF and the reductant used to support NDP reduction. Our studies show that apo-/mismetalated forms of NrdF can be separated from holo-protein, yielding Mn^{III}_2-Y· NrdF with 1 Y·/β_2 and 4 Mn/β_2. Contrary to our expectations, the purity of Me^{III}_2-Y· NrdF was only a minor factor in activity enhancement (Table 2). Rather, the identity of the reductant used to support turnover was the major limiting factor in obtaining highly active RNR from *B. subtilis*.[9] The optimum endogenous reducing system was TR/TRR/NADPH, which supported catalytic activity of ∼1450 U/mg. However, the major contributor to high enzymatic activity may vary from species to species, given that with *B. anthracis*, Trx1 and DTT yielded similar activities using poorly loaded Mn^{III}_2-NrdF.[25] The basis for the low activity in the *B. anthracis* system is likely associated with mismetalated NrdFs which interfere with formation of an active RNR complex.

The availability of highly active *B. subtilis* NrdF and NrdE have allowed us to assemble an active RNR with a 1:1 ratio of subunits and to analyze the resulting activity in physiological concentration ranges (Figure 4). The K_m of 0.025 μM contrasts with values of ∼0.2 μM measured for the Ia RNR subunits, in which each subunit is assayed independently in the presence of a 5−10-fold excess of the second subunit to generate the "active" complex.[13,14] All the assays on the *B. anthracis* RNR were carried out using the class Ia method.[24,25] These conditions could alter quaternary structures (α and α/β structures) and result in inhibition under these assay conditions (see discussion below). With bacterial systems, we now believe that all assays of enzymatic activity should be carried out with a 1:1 ratio of the two subunits, accompanied by a study to establish the optimum concentration range for maximum active complex formation with each RNR.

Two issues warrant further discussion of our results with *B. subtilis* in comparison those with *B. anthracis* (and *B. cereus*) Ib RNRs: the nature of the endogenous reductant(s)[24,25] and the nature and dynamics of their quaternary structure(s). In the studies of Gustafsson et al., interrogation of the *B. anthracis* genome identified three thioredoxins, two potential thioredoxin reductases, and three potential glutaredoxin-like proteins all of which were cloned, expressed, and screened for their ability to support RNR activity.[25] The turnover numbers for the *B. anthracis* RNR were highest with Trx1/TR1 and 7-fold greater than with NrdH/TR1 (Supporting Information, SI-Table 1). Furthermore, under their growth conditions, Western analysis revealed that Trx1 was the predominant RNR reductant in the cell.[25]

We used the *B. anthracis* genes[25] as queries of the *B. subtilis* genome and identified six thioredoxin-like proteins (TrxA, Ydbp, YtpP, YdfQ, YusE, and YusI), one thioredoxin reductase (TrxB), and two glutaredoxin-like proteins (YosR and BdbA). TrxA and TrxB are homologues of *B. anthracis* Trx1 (75% identity) and TR1 (87% identity), suggesting they likely function as the reducing system for the *B. subtilis* RNR. In addition, previous gene knock-out experiments of all of these proteins and the growth of the resulting deletion mutants in rich or minimal medium revealed that only TrxA and TrxB are essential.[10,56] Using these purified proteins, we established that endogenous reductants effect a ∼10-fold increase on RNR activity relative to DTT (Table 1) in contrast with the *B. anthracis* RNR.[25] We also note that we have observed a 20-fold difference between endogenous reductant and DTT with the *S. sanguinis* class Ib RNR.[53]

It was pointed out previously that *B. subtilis* has a second class Ib RNR, located in the *bnrdEFI* operon, which could potentially be physiologically important.[24] The gene *yosR*, recently reannotated as *nrdH*, is adjacent to this operon,[25,54] prompting us to examine this protein in our assays as well. As was observed with the *B. anthracis* RNR, YosR(NrdH) exhibits activity similar to TrxA in ribonucleotide reduction (Table 1). In *B anthracis*, as noted above, Western analysis suggested that TrxA was the endogenous reductant. Previous studies in *B. subtilis* have established that the *bnrdEFI* operon is dispensable for its survival under numerous growth conditions,[11,12,57] supported by transcriptional analysis under rich and minimal growth conditions in which both *yosR* and *bnrdEFI* were expressed at very low levels.[58] Thus, TrxA is most likely the physiological reductant in *B. subtilis* as well.

The most interesting observation from our studies is associated with our analysis of quaternary structure. We expected tight subunit association in the absence of nucleotides (dNTPs), based on our isolation of endogenous *B. subtilis* RNR[9] and the concentration dependence of activity (Figure 4), in contrast to the class Ia RNRs (K_d of 0.4 μM).[14,59] Our studies using SEC and SV-AUC, however, revealed that this is not the case (Figure 5). Under physiological concentrations (1 μM) with no nucleotides, both methods revealed mixtures of subunits and complexes of subunits. GEMMA analysis of the *B. anthracis* class Ib RNR in the absence of nucleotides also revealed mixtures of subunits and an $\alpha_2\beta_2$ complex.[24] In neither our case, nor in the case of these earlier studies, however has a study of affinities and the rates for subunit association and dissociation been carried out.

Finally, the observation of potent inhibition of RNR activity by dATP given the absence of an ATP cone domain deserves comment. The results are distinct from all class Ib RNRs reported to date, which show no inhibition even at concentrations of 1 mM dATP.[5,49,50,53,60] Furthermore, with dATP and the *B. anthracis* RNR, the GEMMA analysis revealed individual subunits, $\alpha\beta_2$, and $\alpha_2\beta_2$, but no large quaternary states were reported.[24] Thus, the cause for the potent inhibition with the *B. subtilis* RNR requires further study.

Our studies[16,17,22] suggest that the paradigm of RNR as $\alpha_2\beta_2$ in the literature needs to be re-examined. The difficulties associated with obtaining structures of prokaryotic RNRs with both subunits present are likely associated with the dynamics of

their interactions. Undoubtedly these dynamics will be affected by the presence of ATP, dNTPs, and Mg^{2+}, and studies of these effects under physiologically relevant conditions are currently in progress. In order to carry out these types of studies, highly active protein with fully loaded metallo-cofactor is essential, and our studies reported herein present the foundation to investigate quaternary structure and its connection to the enzymatic activity and allosteric regulation of RNRs.

■ ASSOCIATED CONTENT

Supporting Information

Experimental details of NrdE purification, SDS-PAGE densitometry, and hydrodynamic property predictions; detailed results of SV-AUC experiments; TrxA, TrxB, and YosR cloning primers and purity analyses; spectroscopic characterization of apo-/mismetalated and holo-Me^{III}_2-Y· NrdF isolated from MonoQ anion exchange; and SV-AUC concentration sedimentation coefficient distributions. This material is available free of charge via the Internet at http://pubs.acs.org.

■ AUTHOR INFORMATION

Corresponding Author

*E-mail: stubbe@mit.edu. Tel.: (617) 253-1814. Fax: (617) 258-7247.

Present Address

[#]Harvard Medical School, Department of Microbiology and Immunobiology, 77 Avenue Louis Pasteur, Boston, MA 02115.

Funding

This work was supported by the National Institute of Health Grant GM81393 to J.S.

Notes

The authors declare no competing financial interest.

■ ACKNOWLEDGMENTS

The Biophysical Instrumentation Facility for the Study of Complex Macromolecular Systems (NSF-007031) is gratefully acknowledged, in particular, D. Pheasant for technical assistance with the AUC experiments. We thank N. Ando and M. Gibson (C. Drennan laboratory) and A. Wommack (E. Nolan laboratory) for helpful discussion and assistance with AUC data processing and analysis. We wish to thank S. J. Lippard for use of his atomic absorption spectrometer and J. Wilson of the Lippard lab for assistance in data acquisition.

■ ABBREVIATIONS

dATP, deoxyadenosine 5′-triphosphate; ATP, adenosine 5′-triphosphate; BCA, bicinchoninic acid; BSA, bovine serum albumin; CDP, cytidine 5′-diphosphate; CV, column volume; dNDPs, deoxyribonucleoside 5′-diphosphates; dNTPs, deoxyribonucleoside 5′-triphoshpates; DTNB, 5,5′-dithiobis-(2-nitrobenzoic acid); DTT, dithiothreitol; EDTA, ethylenediaminetetraacetic acid; EPR, electron paramagnetic resonance; FAD, flavin adenine dinucleotide; HEPES, *N*-2-hydroxyethylpiperazine-*N*-2′-ethanesulfonic acid; IPTG, isopropyl-*β*-D-thiogalactoside; NADPH, nicotinamide adenine dinucleotide phosphate; NaP_i, sodium phosphate; NDPs, ribonucleoside-5′-diphosphates; Ni-NTA, nickel nitrilotriacetic acid; SDS-PAGE, sodium dodecyl sulfate-polyacrylamide gel electrophoresis; SEC, size exclusion chromatography; SV-AUC, sedimentation velocity analytical ultracentrifugation; TCEP, tris(2-carboxyethyl)phosphine; TR, thioredoxin; Tris, Tris-(hydroxyethyl)amino methane; TRR, thioredoxin reductase; Y·, tyrosyl radical

■ ADDITIONAL NOTE

[a]The reported activity of the *C. ammoniagenes* class Ib RNR[8] is inconsistent with activities of all known RNRs and is likely incorrect.

■ REFERENCES

(1) Hofer, A., Crona, M., Logan, D. T., and Sjöberg, B. M. (2012) DNA Building Blocks: Keeping Control of Manufacture. *Crit. Rev. Biochem. Mol. Biol. 47*, 50−63.

(2) Cotruvo, J. A., and Stubbe, J. (2011) Class I Ribonucleotide Reductases: Metallocofactor Assembly and Repair *in vitro* and *in vivo*. *Annu. Rev. Biochem. 80*, 733−767.

(3) Eliasson, R., Pontis, E., Jordan, A., and Reichard, P. (1996) Allosteric Regulation of the Third Ribonucleotide Reductase (NrdEF Enzyme) from Enterobacteriaceae. *J. Biol. Chem. 271*, 26582−26587.

(4) Huque, Y., Fieschi, F., Torrents, E., Gibert, I., Eliasson, R., Reichard, P., Sahlin, M., and Sjöberg, B. M. (2000) The Active Form of the R2F Protein of Class Ib Ribonucleotide Reductase from *Corynebacterium ammoniagenes* is a Diferric Protein. *J. Biol. Chem. 275*, 25365−25371.

(5) Jordan, A., Pontis, E., Atta, M., Krook, M., Gibert, I., Barbé, J., and Reichard, P. (1994) A Second Class I Ribonucleotide Reductase in Enterobacteriaceae - Characterization of the *Salmonella typhimurium* Enzyme. *Proc. Natl. Acad. Sci. U. S. A. 91*, 12892−12896.

(6) Cotruvo, J. A., and Stubbe, J. (2011) *Escherichia coli* Class Ib Ribonucleotide Reductase Contains a Dimanganese(III)-Tyrosyl Radical Cofactor *in vivo*. *Biochemistry 50*, 1672−1681.

(7) Cox, N., Ogata, H., Stolle, P., Reijerse, E., Auling, G., and Lubitz, W. (2010) A Tyrosyl-Dimanganese Coupled Spin System is the Native Metalloradical Cofactor of the R2F Subunit of the Ribonucleotide Reductase of *Corynebacterium ammoniagenes*. *J. Am. Chem. Soc. 132*, 11197−11213.

(8) Stolle, P., Barckhausen, O., Oehlmann, W., Knobbe, N., Vogt, C., Pierik, A. J., Cox, N., Schmidt, P. P., Reijerse, E. J., Lubitz, W., and Auling, G. (2010) Homologous Expression of the *nrdF* Gene of *Corynebacterium ammoniagenes* Strain ATCC 6872 Generates a Manganese-metallocofactor (R2F) and a Stable Tyrosyl Radical (Y·) Involved in Ribonucleotide Reduction. *FEBS J. 277*, 4849−4862.

(9) Zhang, Y., and Stubbe, J. (2011) *Bacillus subtilis* Class Ib Ribonucleotide Reductase is a Dimanganese(III)-Tyrosyl Radical Enzyme. *Biochemistry 50*, 5615−5623.

(10) Kobayashi, K., Ehrlich, S. D., Albertini, A., Amati, G., Andersen, K. K., Arnaud, M., Asai, K., Ashikaga, S., Aymerich, S., Bessieres, P., Boland, F., Brignell, S. C., Bron, S., Bunai, K., Chapuis, J., Christiansen, L. C., Danchin, A., Débarbouillé, M., Dervyn, E., Deuerling, E., Devine, K., Devine, S. K., Dreesen, O., Errington, J., Fillinger, S., Foster, S. J., Fujita, Y., Galizzi, A., Gardan, R., Eschevins, C., Fukushima, T., Haga, K., Harwood, C. R., Hecker, M., Hosoya, D., Hullo, M. F., Kakeshita, H., Karamata, D., Kasahara, Y., Kawamura, F., Koga, K., Koski, P., Kuwana, R., Imamura, D., Ishimaru, M., Ishikawa, S., Ishio, I., Le Coq, D., Masson, A., Mauël, C., Meima, R., Mellado, R. P., Moir, A., Moriya, S., Nagakawa, E., Nanamiya, H., Nakai, S., Nygaard, P., Ogura, M., Ohanan, T., O'Reilly, M., O'Rourke, M., Pragai, Z., Pooley, H. M., Rapoport, G., Rawlins, J. P., Rivas, L. A., Rivolta, C., Sadaie, A., Sadaie, Y., Sarvas, M., Sato, T., Saxild, H. H., Scanlan, E., Schumann, W., Seegers, J., Sekiguchi, J., Sekowska, A., Séror, S. J., Simon, M., Stragier, P., Studer, R., Takamatsu, H., Tanaka, T., Takeuchi, M., Thomaides, H. B., Vagner, V., van Dijl, J. M., Watabe, K., Wipat, A., Yamamoto, H., Yamamoto, M., Yamamoto, Y., Yamane, K., Yata, K., Yoshida, K., Yoshikawa, H., Zuber, U., and Ogasawara, N. (2003) Essential *Bacillus subtilis* Genes. *Proc. Natl. Acad. Sci. U. S. A. 100*, 4678−4683.

(11) Lazarevic, V., Soldo, B., Düsterhöft, A., Hilbert, H., Mauël, C., and Karamata, D. (1998) Introns and Intein Coding Sequence in the Ribonucleotide Reductase Genes of *Bacillus subtilis* Temperate Bacteriophage SP*β*. *Proc. Natl. Acad. Sci. U. S. A. 95*, 1692−1697.

(12) Westers, H., Dorenbos, R., van Dijl, J. M., Kabel, J., Flanagan, T., Devine, K. M., Jude, F., Séror, S. J., Beekman, A. C., Darmon, E., Eschevins, C., de Jong, A., Bron, S., Kuipers, O. P., Albertini, A. M., Antelmann, H., Hecker, M., Zamboni, N., Sauer, U., Bruand, C., Ehrlich, D. S., Alonso, J. C., Salas, M., and Quax, W. J. (2003) Genome Engineering Reveals Large Dispensable Regions in *Bacillus subtilis*. *Mol. Biol. Evol. 20*, 2076−2090.
(13) Climent, I., Sjöberg, B. M., and Huang, C. Y. (1991) Carboxyl-Terminal Peptides as Probes for *Escherichia coli* Ribonucleotide Reductase Subunit Interaction - Kinetic Analysis of Inhibition Studies. *Biochemistry 30*, 5164−5171.
(14) Hassan, A. Q., Wang, Y. T., Plate, L., and Stubbe, J. (2008) Methodology To Probe Subunit Interactions in Ribonucleotide Reductases. *Biochemistry 47*, 13046−13055.
(15) Ingemarson, R., and Thelander, L. (1996) A Kinetic Study on the Influence of Nucleoside Triphosphate Effectors on Subunit Interaction in Mouse Ribonucleotide Reductase. *Biochemistry 35*, 8603−8609.
(16) Ando, N., Brignole, E. J., Zimanyi, C. M., Funk, M. A., Yokoyama, K., Asturias, F. J., Stubbe, J., and Drennan, C. L. (2011) Structural Interconversions Modulate Activity of *Escherichia coli* Ribonucleotide Reductase. *Proc. Natl. Acad. Sci. U. S. A. 108*, 21046−21051.
(17) Minnihan, E. C., Ando, N., Brignole, E. J., Olshansky, L., Chittuluru, J., Asturias, F. J., Drennan, C. L., Nocera, D. G., and Stubbe, J. (2013) Generation of a Stable, Aminotyrosyl Radical-Induced $\alpha_2\beta_2$ Complex of *Escherichia coli* Class Ia Ribonucleotide Reductase. *Proc. Natl. Acad. Sci. U. S. A. 110*, 3835−3840.
(18) Rofougaran, R., Crona, M., Vodnala, M., Sjöberg, B. M., and Hofer, A. (2008) Oligomerization Status Directs Overall Activity Regulation of the *Escherichia coli* Class Ia Ribonucleotide Reductase. *J. Biol. Chem. 283*, 35310−35318.
(19) Kashlan, O. B., Scott, C. P., Lear, J. D., and Cooperman, B. S. (2002) A Comprehensive Model for the Allosteric Regulation of Mammalian Ribonucleotide Reductase. Functional Consequences of ATP- and dATP-induced Oligomerization of the Large Subunit. *Biochemistry 41*, 462−474.
(20) Rofougaran, R., Vodnala, M., and Hofer, A. (2006) Enzymatically Active Mammalian Ribonucleotide Reductase Exists Primarily as an $\alpha_6\beta_2$ Octamer. *J. Biol. Chem. 281*, 27705−27711.
(21) Fairman, J. W., Wijerathna, S. R., Ahmad, M. F., Xu, H., Nakano, R., Jha, S., Prendergast, J., Welin, R. M., Flodin, S., Roos, A., Nordlund, P., Li, Z., Walz, T., and Dealwis, C. G. (2011) Structural Basis for Allosteric Regulation of Human Ribonucleotide Reductase by Nucleotide-induced Oligomerization. *Nat. Struct. Mol. Biol. 18*, 316−322.
(22) Zimanyi, C. M., Ando, N., Brignole, E. J., Asturias, F. J., Stubbe, J., and Drennan, C. L. (2012) Tangled Up in Knots: Structures of Inactivated Forms of *E. coli* Class Ia Ribonucleotide Reductase. *Structure 20*, 1374−1383.
(23) Crona, M., Furrer, E., Torrents, E., Edgell, D. R., and Sjöberg, B. M. (2010) Subunit and Small Molecule Interaction of Ribonucleotide Reductases via Surface Plasmon Resonance Biosensor Analyses. *Protein Eng. Des. Sel. 23*, 633−641.
(24) Crona, M., Torrents, E., Røhr, A. K., Hofer, A., Furrer, E., Tomter, A. B., Andersson, K. K., Sahlin, M., and Sjöberg, B. M. (2011) NrdH-Redoxin Protein Mediates High Enzyme Activity in Manganese-reconstituted Ribonucleotide Reductase from *Bacillus anthracis*. *J. Biol. Chem. 286*, 33053−33060.
(25) Gustafsson, T. N., Sahlin, M., Lu, J., Sjöberg, B. M., and Holmgren, A. (2012) *Bacillus anthracis* Thioredoxin Systems, Characterization and Role as Electron Donors for Ribonucleotide Reductase. *J. Biol. Chem. 287*, 39686−39697.
(26) Ge, J., Yu, G. X., Ator, M. A., and Stubbe, J. (2003) Pre-Steady-state and Steady-state Kinetic Analysis of *E. coli* Class I Ribonucleotide Reductase. *Biochemistry 42*, 10071−10083.
(27) Cotruvo, J. A., Stich, T. A., Britt, R. D., and Stubbe, J. (2013) Mechanism of Assembly of the Dimanganese-Tyrosyl Radical Cofactor of Class Ib Ribonucleotide Reductase: Enzymatic Generation of Superoxide is Required for Tyrosine Oxidation via an Mn(III)Mn(IV) Intermediate. *J. Am. Chem. Soc. 135*, 4027−4039.
(28) Cotruvo, J. A., and Stubbe, J. (2008) NrdI, a Flavodoxin Involved in Maintenance of the Diferric-Tyrosyl Radical Cofactor in *Escherichia coli* Class Ib Ribonucleotide Reductase. *Proc. Natl. Acad. Sci. U. S. A. 105*, 14383−14388.
(29) Moore, E. C., Reichard, P., and Thelander, L. (1964) Enzymatic Synthesis of Deoxyribonucleotides. V. Purification and Properties of Thioredoxin Reductase from *Escherichia coli* B. *J. Biol. Chem. 239*, 3445−3452.
(30) Thelander, L. (1967) Thioredoxin Reductase - Characterization of a Homogeneous Preparation from *Escherichia coli* B. *J. Biol. Chem. 242*, 852−859.
(31) Smith, P. K., Krohn, R. I., Hermanson, G. T., Mallia, A. K., Gartner, F. H., Provenzano, M. D., Fujimoto, E. K., Goeke, N. M., Olson, B. J., and Klenk, D. C. (1985) Measurement of Protein Using Bicinchoninic Acid. *Anal. Biochem. 150*, 76−85.
(32) Prongay, A. J., Engelke, D. R., and Williams, C. H. (1989) Characterization of Two Active-Site Mutations of Thioredoxin Reductase from *Escherichia coli*. *J. Biol. Chem. 264*, 2656−2664.
(33) Fish, W. W. (1988) Rapid Colorimetric Micromethod for the Quantitation of Complexed Iron in Biological Samples. *Method Enzymol. 158*, 357−364.
(34) Cotruvo, J. A., and Stubbe, J. (2010) An Active Dimanganese-(III)-Tyrosyl Radical Cofactor in *Escherichia coli* Class Ib Ribonucleotide Reductase. *Biochemistry 49*, 1297−1309.
(35) Steeper, J. R., and Steuart, C. D. (1970) A Rapid Assay for CDP Reductase Activity in Mammalian Cell Extracts. *Anal. Biochem. 34*, 123−130.
(36) Siegel, L. M., and Monty, K. J. (1966) Determination of Molecular Weights and Frictional Ratios of Proteins in Impure Systems by Use of Gel Filtration and Density Gradient Centrifugation. Application to Crude Preparations of Sulfite and Hydroxylamine Reductases. *Biochim. Biophys. Acta 112*, 346−362.
(37) Laurent, T. C., and Killander, J. (1964) Theory of Gel Filtration and its Experimental Verification. *J. Chromatogr. 14*, 317−330.
(38) Meirelles, G. V., Silva, J. C., Mendonca, Y. D., Ramos, C. H. I., Torriani, I. L., and Kobarg, J. (2011) Human Nek6 is a Monomeric Mostly Globular Kinase with an Unfolded Short N-terminal Domain. *BMC Struct. Biol. 11*, 12.
(39) Zhao, H. Y., Ghirlando, R., Piszczek, G., Curth, U., Brautigam, C. A., and Schuck, P. (2013) Recorded Scan Times can Limit the Accuracy of Sedimentation Coefficients in Analytical Ultracentrifugation. *Anal. Biochem. 437*, 104−108.
(40) Balbo, A., and Schuck, P. (2005) Analytical Ultracentrifugation in the Study of Protein Self-association and Heterogeneous Protein-Protein Interactions, In *Protein-Protein Interactions: A Molecular Cloning Manual* (Golemis, E. A., and Adams, P. D., Eds.), pp 253−277, Cold Spring Harbor Laboratory Press, New York.
(41) Schuck, P. (2003) On the Analysis of Protein Self-association by Sedimentation Velocity Analytical Ultracentrifugation. *Anal. Biochem. 320*, 104−124.
(42) Laue, T. M., Shah, B. D., Ridgeway, T. M., and Pelletier, S. L. (1992) Computer-aided Interpretation of Analytical Sedimentation Data for Proteins, In *Analytical Ultracentrifugation in Biochemistry and Polymer Science* (Harding, S. E., Rowe, A. J., and Horton, J. C., Eds.) pp 90−125, Royal Society of Chemistry, Cambridge.
(43) Ortega, A., Amorós, D., and de la Torre, J. G. (2011) Prediction of Hydrodynamic and Other Solution Properties of Rigid Proteins from Atomic- and Residue-Level Models. *Biophys. J. 101*, 892−898.
(44) Boal, A. K., Cotruvo, J. A., Stubbe, J., and Rosenzweig, A. C. (2012) The Dimanganese(II) Site of *Bacillus subtilis* Class Ib Ribonucleotide Reductase. *Biochemistry 51*, 3861−3871.
(45) Kelley, L. A., and Sternberg, M. J. E. (2009) Protein Structure Prediction on the Web: A Case Study Using the Phyre Server. *Nat. Protoc. 4*, 363−371.
(46) Uppsten, M., Färnegårdh, M., Jordan, A., Eliasson, R., Eklund, H., and Uhlin, U. (2003) Structure of the Large Subunit of Class Ib

Ribonucleotide Reductase from *Salmonella typhimurium* and its Complexes with Allosteric Effectors. *J. Mol. Biol. 330*, 87−97.
(47) Jordan, A., Aslund, F., Pontis, E., Reichard, P., and Holmgren, A. (1997) Characterization of *Escherichia coli* NrdH - A Glutaredoxin-like Protein with a Thioredoxin-like Activity Profile. *J. Biol. Chem. 272*, 18044−18050.
(48) Thelander, L., Sjöberg, B. R., and Eriksson, S. (1978) Ribonucleoside Diphosphate Reductase (*Escherichia coli*). *Method Enzymol. 51*, 227−237.
(49) Yang, F. D., Curran, S. C., Li, L. S., Avarbock, D., Graf, J. D., Chua, M. M., Lui, G. Z., Salem, J., and Rubin, H. (1997) Characterization of Two Genes Encoding the *Mycobacterium tuberculosis* Ribonucleotide Reductase Small Subunit. *J. Bacteriol. 179*, 6408−6415.
(50) Jordan, A., Pontis, E., Aslund, F., Hellman, U., Gibert, I., and Reichard, P. (1996) The Ribonucleotide Reductase System of *Lactococcus lactis* - Characterization of an NrdEF Enzyme and a New Electron Transport Protein. *J. Biol. Chem. 271*, 8779−8785.
(51) Uppsten, M., Färnegårdh, M., Domkin, V., and Uhlin, U. (2006) The First Holocomplex Structure of Ribonucleotide Reductase Gives New Insight into its Mechanism of Action. *J. Mol. Biol. 359*, 365−377.
(52) Uhlin, U., and Eklund, H. (1994) Structure of Ribonucleotide Reductase Protein R1. *Nature 370*, 533−539.
(53) Makhlynets, O., Boal, A. K., Rhodes, D. V., Kitten, T., Rosenzweig, A. C., and Stubbe, J. (2013) *Streptococcus sanguinis* Class Ib Ribonucleotide Reductase: High Activity with Both Iron and Manganese Cofactors and Structural Insights. *J. Biol. Chem.* DOI: 10.1074/jbc.M113.533554.
(54) Lundin, D., Torrents, E., Poole, A. M., and Sjöberg, B. M. (2009) RNRdb, a Curated Database of the Universal Enzyme Family Ribonucleotide Reductase, Reveals a High Level of Misannotation in Sequences Deposited to Genbank. *BMC Genomics 10*, 589.
(55) Bollinger, J. M., Jr. (1993) On the Chemical Mechanism of Assembly of the Tyrosyl Radical-Dinuclear Iron Cluster Cofactor of *E. coli* Ribonucleotide Reductase, Ph.D. Dissertation, Massachusetts Institute of Technology, Cambridge, MA.
(56) Smits, W. K., Dubois, J. Y. F., Bron, S., van Dijl, J. M., and Kuipers, O. P. (2005) Tricksy Business: Transcriptome Analysis Reveals the Involvement of Thioredoxin A in Redox Homeostasis, Oxidative Stress, Sulfur Metabolism, and Cellular Differentiation in *Bacillus subtilis*. *J. Bacteriol. 187*, 3921−3930.
(57) Härtig, E., Hartmann, A., Schätzle, M., Albertini, A. M., and Jahn, D. (2006) The *Bacillus subtilis nrdEF* Genes, Encoding a Class Ib Ribonucleotide Reductase, are Essential for Aerobic and Anaerobic Growth. *Appl. Environ. Microbiol. 72*, 5260−5265.
(58) Rasmussen, S., Nielsen, H. B., and Jarmer, H. (2009) The Transcriptionally Active Regions in the Genome of *Bacillus subtilis*. *Mol. Microbiol. 73*, 1043−1057.
(59) Brown, N. C., and Reichard, P. (1969) Ribonucleoside Diphosphate Reductase - Formation of Active and Inactive Complexes of Proteins B1 and B2. *J. Mol. Biol. 46*, 25−38.
(60) Roca, I., Torrents, E., Sahlin, M., Gibert, I., and Sjöberg, B. M. (2008) NrdI Essentiality for Class Ib Ribonucleotide Reduction in *Streptococcus pyogenes*. *J. Bacteriol. 190*, 4849−4858.

■ NOTE ADDED AFTER ASAP PUBLICATION

This article was published ASAP on January 21, 2014, with minor errors in Table 2. The corrected version was published ASAP on January 22, 2014.